Mon. Not. R. Astron. Soc. **000**, 1–18 (2002) Printed 9 March 2012 (MN LATEX style file v2.2)

Holographic imaging of crowded fields: an effective poor man's adaptive optics system

R. Schödel[1⋆], S. Yelda[2], A. Ghez[2], J. H. V. Girard[3], L. Labadie[4], R. Rebolo[5], A. Pérez-Garrido[6], M.R.Morris[2]

[1] *Instituto de Astrofísica de Andalucía (CSIC), Glorieta de la Astronomía S/N, 18008 Granada, Spain*
[2] *Department of Physics and Astronomy, UCLA, Los Angeles, CA 90095-1547, USA*
[3] *European Southern Observatory (ESO), Casilla 19001, Vitacura, Santiago, Chile*
[4] *I.Physikalisches Institut, Universität zu Köln, Zülpicher Str. 77, 50937Köln, Germany*
[5] *Instituto de Astrofísica de Canarias, C/ Vía Láctea s/n, La Laguna, Tenerife E-38200, Spain*
[6] *Universidad Politécnica de Cartagena, Campus Muralla del Mar, Cartagena, E-30202, Spain*

ABSTRACT

We present a method for speckle holography that is optimised for crowded fields. Its two key features are an iterative improvement of the instantaneous PSFs extracted from each speckle frame and the (optional) simultaneous use of multiple reference stars. In this way, high signal-to-noise and accuracy be achieved on the PSFs for each short exposure, which results in sensitive, high-Strehl reconstructed images. We have tested our method with different instruments, on a range of targets, and from the $N-$ to the I-band. In terms of PSF cosmetics and stability as well as Strehl ratio, holographic imaging can be equal, or even superior, to the capabilities of currently available AO systems. It outperforms lucky imaging because it makes use of the entire PSF and reduces the need for frame selection, thus leading to higher Strehl and improved sensitivity. Image reconstruction a posteriori, the possibility to use multiple reference stars and the fact that these reference stars can be rather faint means that holographic imaging offers a simple way to image large, dense stellar fields near the diffraction limit of large telescopes, similar to the capabilities of a multi-conjugate adaptive optics systems. Although sensitivity is limited because of the necessary short exposure times, this limitation is not severe (e.g., a $5\,\sigma$ point source sensitivity of $Ks \approx 19$ was reached in 0.5 h of observing time with NaCo/VLT). Our work opens new possibilities for sub-arcsecond resolution imaging of large crowded fields with high PSF stability, while keeping the complexity and costs of instruments small. Moreover, the presented method can be used to significantly improve the angular resolution of any existing imaging instrument that provides sufficiently fine spatial sampling and fast readout capability. Holography can also be combined with AO imaging to improve performance in case of unstable seeing or observations at short wavelengths. While use of AO is necessary to image faint targets, perform high angular resolution spectroscopy, or observe isolated objects, holography can provide unique advantages for imaging of large fields, of highly extincted targets, or at short infrared to optical wavelengths.

Key words: high resolution imaging

1 INTRODUCTION

Obtaining images at or near the diffraction limit of 4-10m class telescopes from the ground is key to many astrophysical projects, like investigating the structure and dynamics of globular clusters or of the Galaxy's nuclear star cluster, the multiplicity of massive stars, or the direct detection of planets and circumstellar discs. Before the end of the 1990s, this goal was generally reached by speckle imaging. The technique of speckle interferometry is based on recording long series of short exposure images, with integration times usually on the order of the atmospheric coherence time, and digital image reconstruction *a posteriori* using a range of different techniques (e.g., Labeyrie 1970; Knox 1976; Weigelt

⋆ E-mail:rainer@iaa.es

1977; Lohmann et al. 1983; Christou et al. 1987; Christou 1991). Speckle imaging has led to fundamental scientific discoveries like the measurement of the orbits of stars around the massive black hole at the center of the Milky Way (Ghez et al. 2000; Eckart et al. 2002; Schödel et al. 2003; Ghez et al. 2005) or the discovery that at least 50% of O/B stars are multiple (e.g., Mason et al. 2009; Maíz Apellániz 2010).

In the past two decades adaptive optics (AO) assisted observations have become the standard for obtaining near-infrared images of near the diffraction limit of large telescopes. In AO imaging, a bright guide star or an artificial laser guide star are used as reference to calculate the deformation of the incoming wavefront. The wavefront is subsequently (partially) corrected with the help of a deformable mirror before the light is registered by the detector. An example of such an AO assisted system is CONICA/NAOS (NaCo) at the 8m-class ESO VLT (Lenzen et al. 2003; Rousset et al. 2003). AO assisted imaging has several important advantages over speckle imaging. For example, long integration times significantly increase the sensitivity of the images, that are limited by the sky brightness in AO imaging, not by detector readout noise as in the case of speckle imaging. AO imaging also makes it possible to use special observing techniques like coronagraphy or spectroscopy.

However, in spite of the enormous success of AO instrumentation, the technique is not perfect. Typical sources of systematic errors are the finite spatial bandwidth due to, e.g. a finite number of sub-apertures in the wavefront sensor as well as a deformable mirror with a finite number of actuators, or leakage of high spatial frequency errors due to the limitations imposed by actuator spacing on the deformable mirror. These effects lead to difficulties in calibrating the AO PSF and detecting structure or point sources within a few FWHM of the PSF (Tuthill et al. 2006). Another difficulty is that the PSF of an AO image varies systematically across the field-of-view (FOV) and that the Strehl ratio deteriorates rapidly with increasing distance from the guide star. These *anisoplanatic* effects result because different viewing directions probe different turbulence profiles of the atmosphere, but a single-conjugated AO system only corrects the turbulence profile toward the guide star.

Various solutions to the described problems have been developed, like AO assisted sparse aperture masking (Tuthill et al. 2006; Lacour et al. 2011) or multi-conjugate adaptive optics (e.g. Rigaut et al. 2000). In addition, the use of laser guide stars (LGSs) frees AO systems from the requirement of having bright stars close to the target. However, all these solutions come at a price. The increased technical complexity is inevitably accompanied by exploding costs and increased vulnerability of the systems. It is therefore important to keep exploring the possibilities of speckle imaging, which can be sufficient for many science cases, at much reduced cost and increased robustness. For example, speckle imaging has recently experienced a renaissance at optical wavelengths in the form of *lucky imaging* (e.g., Hormuth et al. 2008; Labadie et al. 2003).

In this paper we describe a new implementation of the so-called *speckle holography* technique that we have tested both by simulations and by observations with a large variety of instruments. While speckle imaging suffers inevitably from a limited sensitivity due to the required short readout times, this limitation is less severe with holographic image reconstruction than with other techniques. Particular advantages of the method introduced here are that it allows to simultaneously use several reference stars and can deal efficiently with anisoplanatic effects in crowded fields.

Since image reconstruction in speckle imaging is performed *a posteriori*, no systematic PSF errors are introduced into the data at the time of recording them. If several sufficiently bright stars are available distributed over the field of view, sub-fields smaller than the isoplanatic angle can be reconstructed from speckle data. In this way, the final image can have significantly reduced anisoplanatic effects.

We have written a program package that provides excellent results based on iteratively improved extraction of the instantaneous PSF from speckle frames and on the optional simultaneous use of multiple guide stars. The algorithm has been specifically developed for crowded fields, but will also work on isolated targets if a reference star (or several ones) is located sufficiently close. Here we show applications of the algorithm to observations of different targets and at various wavelengths, as well as to simulated data. The algorithm shows excellence performance with respect to PSF Strehl and cosmetics, works with faint guide stars, and is more efficient than lucky imaging techniques, which is of great advantage at short NIR to optical wavelengths.

The paper is structured as follows. We give a brief introduction to speckle image reconstruction, followed by a detailed description of our algorithm, that is illustrated by its application to near-infrared speckle data on NGC 3603 obtained with NaCo/VLT. In subsequent sections, we explore the performance of the technique as concerns sensitivity and photometric and astrometric accuracy as well as its application to short-wavelengths ($J-$ and $I-$bands) and to an extremely crowded field (Galactic center). We then continue with a discussion of the problems and merits of the method, and in what situations we recommend the use of the holographic technique. A brief summary closes this article.

2 SPECKLE IMAGE RECONSTRUCTION

A range of different algorithms exists for image reconstruction from speckle data. Bispectrum, or speckle masking, techniques have been frequently used because they can serve to reconstruct an image of complex targets without the necessity of observing an unresolved reference source (e.g., Weigelt 1977; Lohmann et al. 1983; Weigelt et al. 2006). On the downside, bispectrum methods are complex and require considerable amounts computing time. One of the most widely spread ways of reducing speckle data of a large field-of-view containing multiple objects is the so-called simple shift-and-add (SSA) method (e.g., Christou 1991), which has been frequently applied to Galactic center observations (e.g., Eckart & Genzel 1996; Ghez et al. 1998). In a simplified view, each speckle in the instantaneous PSF, or *speckle cloud*, can be regarded as a diffraction limited image of the source. The SSA method consists of applying a different shift to each slice of the data cube before averaging the frames. The individual shifts are given by the offsets of the brightest pixel of the speckle cloud of a reference star from an arbi-

trarily chosen reference position. The PSF of point sources in the resulting image can then be described by the superposition of an airy function over a broad gaussian seeing halo. With this method, typical Strehl ratios of the order 10% can be achieved. Higher values are possible if rigorous frame selection is applied (e.g., Schödel et al. 2003).

The SSA algorithm became so popular because it operates in image space, making Fourier transformations unnecessary, and is therefore very easy to understand, fast, and robust. Edge effects are avoided and the requirements on computing resources are low. SSA has no problems in crowded fields because the brightest speckle of a reference star can usually be identified reliably. However, it uses only a small amount of the available information contained in the image and the majority of the photons of a source end up in the seeing halo.

When combined with rigorous selection of the best frames, SSA can lead to very high Strehl images. This is due to the statistical nature of turbulence, which has the effect that a small percentage of the speckle frames will resemble diffraction limited short exposures, with little distortion by the atmosphere. This method has recently become popular at optical wavelengths, where AO systems still cannot provide satisfactory results, and is termed *lucky imaging* (e.g. Hormuth et al. 2008; Labadie et al. 2003). While working well at small telescopes, lucky imaging becomes increasingly inefficient with larger telescope apertures because the number of speckles increases quadratically with telescope diameter. Thus, it can become necessary to discard $90 - 99\%$ of the data in order to achieve a diffraction limited image.

A more efficient image reconstruction algorithm is the so-called *speckle holography* technique. A concise description of the technique can be found, e.g., in Petr et al. (1998). In brief, the algorithm is a deconvolution technique based on a division of averaged quantities in Fourier space:

$$O = \frac{\langle I_m P_m^* \rangle}{\langle |P_m^2| \rangle}, \quad (1)$$

where O is the Fourier transform of the object, I_m and P_m are the Fourier transforms of the m-th image (speckle frame) and its instantaneous PSF, and the brackets denote the mean over N frames. Taking the average over a large number of frames will effectively suppress the noise. For an infinite number of frames, the denominator is equal to the speckle transfer function related to the turbulence.

It can be shown that equation 1 is the best estimate, in the least squares sense, of the Fourier transform of the object (Primot et al. 1990). This feature of the algorithm allows one to obtain a clean image from the combination of several hundred or thousands of frames. The actual image is obtained after apodizing O with the optical transfer function of the telescope (usually an Airy function) and applying an inverse Fourier transform. The great advantage of speckle holography over the SSA technique is that it uses the *full* information content near the diffraction limit of each short-exposure frame. It thus results in a significantly reduced seeing halos around point-sources and in higher Strehl ratios than the SSA technique. As long as the S/N of the speckle images allows one to identify reliably the reference stars, the Frame selection is not necessary, which leads to a much higher observing efficiency ($\sim$ 100% of frames used) than in the case of lucky imaging ($\sim$ 10% of frames used). This increases the sensitivity and dynamic range of the resulting image.

Key to this technique is a reliable extraction of the instantaneous PSF from each speckle frame. This poses no problem if a bright star is located close enough, i.e. within an isoplanatic angle, of the target and if this star is isolated, i.e. if there are no secondary sources present within the area covered by the speckle clouds. This ideal situation is, however, rather rare, and can be compared to the case of an AO system without a LGS, that has a sky coverage on the order of a few percent (e.g., Rigaut et al. 2000). Also, faint sources will frequently be present close to the reference star and lead to a bias in the extracted instantaneous PSF, which will result in systematic errors, like the presence of negative sources, in the reconstructed image. All of this poses an important obstacles to the application of speckle holography, particularly in crowded fields. Therefore, holography was hardly used before the advent of AO and has hardly ever been used after AO systems became available.

Here, we present an improved algorithm that addresses this key problem of speckle holography via two features: (a) the optional use of several reference stars *simultaneously*, which suppresses systematic errors caused by secondary sources near the reference stars, and (b) an*iterative* approach to PSF extraction, that uses the relative positions and fluxes of sources known from previous image reconstructions for the next iteration. The iterative approach allows us to accurately remove contaminating sources near the reference stars and superpose their images with sub-pixel accuracy to determine the PSF for each speckle frame. The simultaneous use of several reference stars has the additional advantage of increasing the signal-to-noise of the instantaneous PSF and allows one to use a large number of faint reference stars instead of a single, or a few bright ones. Thus, high Strehl ratios can be achieved in the reconstructed images even if there are no bright reference stars available. In conclusion, the improvement to speckle holography presented here essentially concerns the extraction of an accurate instantaneous PSF.

3 METHODOLOGY

Here, we describe the different steps of our image reconstruction process. The algorithm is illustrated by the example of the reduction of speckle data of the core of the dense star cluster NGC 3603, which was observed with NaCo/VLT on 28 January 2010, using the Ks-filter, and the S27 camera. The data were acquired with the so-called *cube mode*, that allows to record fast series of short exposures with a minimal overhead. The AO loop was kept open. Visual seeing was ~ 0.5". Detector windowing was set to 512×514 pixels and the detector integration time (DIT) to 0.11 s, the maximum for this window size. Ten cubes of about 500 frames each were observed, with dithering of a few arcseconds between each series of exposures. Five cubes of a nearby empty field were taken in order to measure the sky background. Sky subtraction, flat-fielding, and interpolation of bad pixels were applied to each short exposure. In total, 4907 pre-processed speckle images were obtained, corresponding to a total integration time on target of 540 s and on sky of $\sim$50 s. An individual speckle frame is shown in the top panel of Fig. 1.

Figure 1. Speckle image reconstruction of Ks-observations of the core of NGC 3603. Top: Image of a single speckle frame. The reference stars used for holographic reconstruction are marked by circles. Middle: SSA image. Bottom: Speckle holographic reconstruction. The reference stars used for the extraction of the instantaneous PSFs are marked in the upper left image. Insets: PSFs of SSA, holographic reconstruction, and of an individual speckle frame. All color scales are logarithmic.

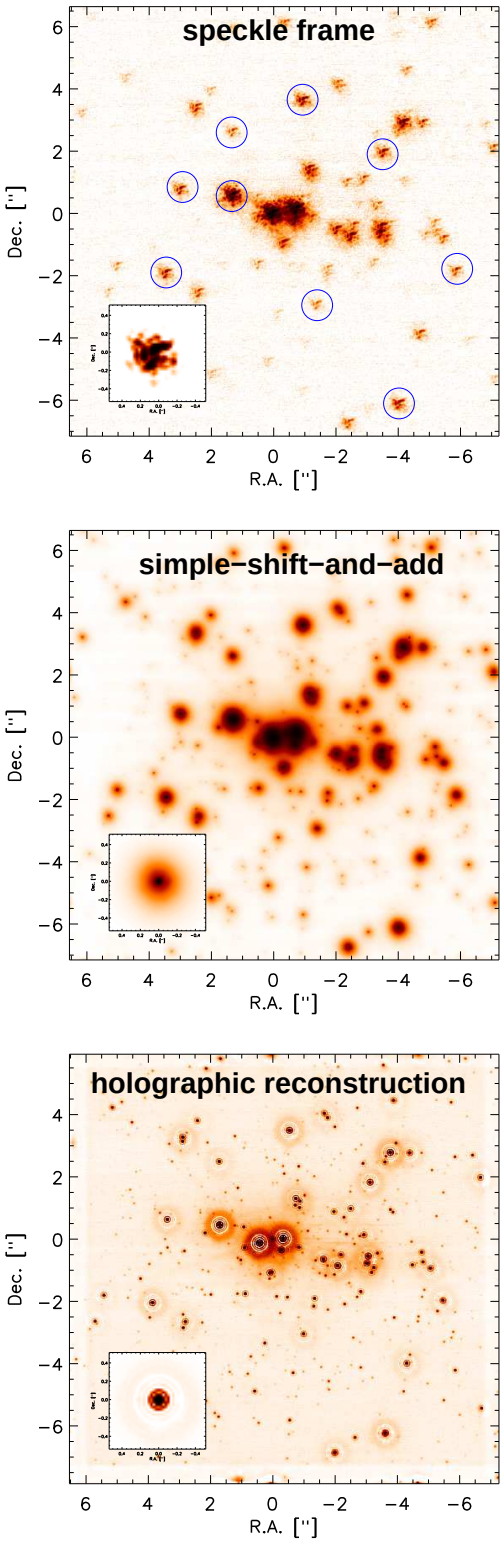

After pre-processing, we proceeded as follows:

(i) Creation of long exposure images for each data cube.

(ii) Pre-alignment of all data cubes. The relative shifts were determined from the centroid of a single bright star in the long-exposures.

(iii) Image reconstruction with the SSA algorithm (middle panel of Fig. 1), using a bright, relatively isolated reference star. Fine-alignment of the speckle frames by using the centroid of the speckle cloud of the reference star.

(iv) PSF fitting astrometry and photometry with *StarFinder* (Diolaiti et al. 2000) on the SSA-image to obtain a preliminary list of positions and fluxes of stars.

(v) Selection of reference stars (blue circles in top panel of Fig. 1) from the list obtained in step (iv).

(vi) Obtain a first estimate of the instantaneous PSF for each speckle frame from the unweighted median of the sub-pixel aligned, flux-normalized images of the reference stars.

(vii) Estimation of noise and background for the PSF from its mean and standard deviation of the pixels in a sufficiently large annulus around the PSF. The additive emission is then subtracted from the PSF estimate and the noise cut is applied by setting all pixels lower than n times the noise to zero (typically, $n = 3$). Finally, a circular mask is applied to the PSF and it is normalized to a total flux of one.

(viii) The preliminary PSF estimate is used to subtract all known secondary, contaminating sources near the reference stars in each frame. Subsequently, an improved PSF estimate is obtained and background subtraction, noise cut, masking, and normalization are applied, as described in the previous step.

(ix) After having determined the PSFs for all speckle frames, the object Fourier transform is estimated by applying equation 1.

(x) Apodisation with the telescope transfer function, TTF, in order to suppress any spatial frequencies above the telescope cutoff-frequency. The TTF is usually an airy function. To estimate the TTF, we have used the routine *strehl* from the ESO software package *eclipse* (Devillard 1997).

(xi) Apply the inverse Fourier transform to obtain the reconstructed image (bottom panel of Fig. 1)).

(xii) Stellar positions and fluxes are measured with *StarFinder* in the reconstructed image, which is of significantly higher quality than the simple shift-and-add image. This means more stars are detected, with greater accuracy of their positions and fluxes. The improved fluxes and positions are then used for a further, final image reconstruction.

Although the mean in equation 1 is very efficient in suppressing random noise, systematic noise is usually present in the raw PSFs that are obtained from a simple median superposition of the reference stars. Sources of such systematic noise can be, e.g. the finite accuracy with which contaminating sources can be subtracted or patterns produced by the detector or readout electronics. For example, faint sources close to the reference stars that are not completely subtracted will cause holes to appear around bright stars in the reconstructed images. Also, an additive offset to the PSF can be caused by smooth, extended emission in the target and must be taken into account. Therefore it is important to apply the background subtraction and noise thresholding described in step (vii).

An individual speckle frame the SSA, and the holo-

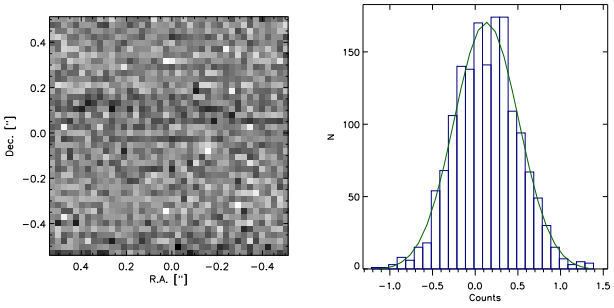

Figure 2. Left: Zoom onto a source-free region in the reconstructed Ks-band image of NGC 3603. Right: Corresponding histogram of pixel values, with Gaussian fit overplotted.

graphically reconstructed images are shown in Fig. 1, along with the corresponding PSFs. The SSA image has an estimated Strehl ratio of ∼9%, while the holographic reconstruction leads to a Strehl ratio of ∼82 ± 5%,. The Strehl and its uncertainty was estimated from three different PSFs created with *StarFinder* using three disjoint sets of reference stars.Due to the noise cut-off applied to the instantaneous PSFs, some of the flux of the stars ends up in circular halos that are visible around bright sources. The noise cut-off would be unnecessary if the reference star(s) were perfectly isolated and there were no source of systematic uncertainties.

There are two novel ideas implemented in our algorithm as compared to previous work with speckle holography (e.g. Petr et al. 1998):

- Iterative approach by using the known relative positions and fluxes of stars from previous image reconstructions to subtract secondary stars close to the reference stars.
- Simultaneous use of several reference stars to create a median PSF.

These innovations allow us to minimize systematic effects due to systematic errors in the estimated instantaneous PSFs. The resulting reconstructed images are of great quality as we show in this and in the following sections.

3.1 Photometry and astrometry

3.1.1 Estimating uncertainties

Holographic image reconstruction (from here on we will simply use the term *holographic imaging*) can be considered a deconvolution technique. Unfortunately, devonvolution can introduce artifacts into images, like the typical ringing around stars in the Wiener deconvolution or the empty spaces around stars and grainy background in the case of the Lucy-Richardson algorithm (see, e.g., Schödel 2010). Additionally, deconvolution procedures can alter the noise statistics by introducing covariances between the pixels and lead to bias in photometry. For example, the Lucy-Richardson method tends to both decompose diffuse emission into point sources and to accumulate diffuse flux around stars into those stars. The latter effect means that the measured flux of ever fainter stars will become increasingly biased if this effect is not taken into account (see Schödel 2010).

Fortunately, speckle holography is (a) a linear algorithm

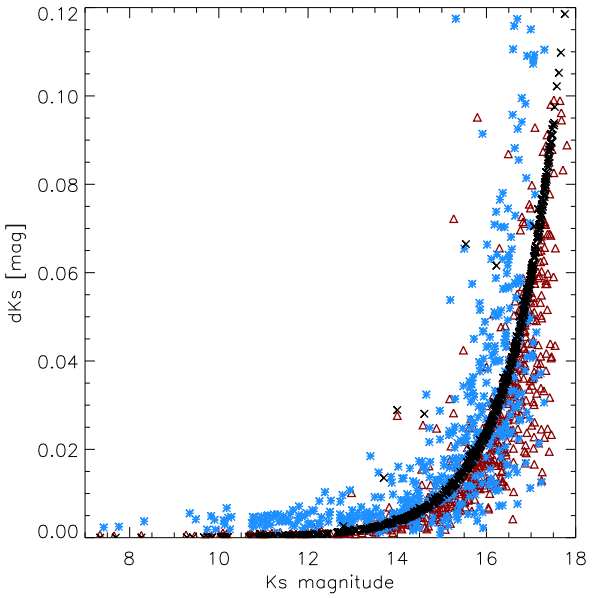

Figure 3. Photometry on the holographically reconstructed Ks-band image of NGC 3603: comparison of different methods to estimate the uncertainties. The black crosses, arranged in a line with very low scatter, represent the formal uncertainties estimated by *StarFinder*, using only gaussian and photon noise estimated with *StarFinder* routines. The blue asterisks show uncertainty estimates from comparing the photometry obtained on images reconstructed from three separate sub-sets of the data. The red rectangles show the formal uncertainties computed by *StarFinder* when using a noise map derived from the images reconstructed from three separate sub-sets of the data.

and (b) a large number of independent frames are averaged before division in Fourier space. While graininess of the background (covariances between pixels) occurs in images reconstructed from a small number of speckle frames, this effect gradually disappears with an increasing number of data. As a rule of thumb reasonable noise statistics will be obtained after averaging several hundred frames. The details depend, of course, on the data set in question. As an example, we show a source-free region of the reconstructed Ks-band image of NGC 3603 in the left panel of Fig. 2 and a histogram of the pixel values plus Gaussian fit in the right panel. There appears to be no obvious cross-correlation between the pixels and the pixel values follow closely a Gaussian distribution.

For astrometry and photometry we used *StarFinder*, a PSF fitting program package, that was specifically developed for the analysis of AO images (Diolaiti et al. 2000). If given a noise map for the image *StarFinder* will calculate the formal uncertainties of the positions and fluxes of point sources. This noise map can be calculated be from the relevant quantities (read-out-noise, dark current, etc.) or directly from the image with the help of *StarFinder* routines, like GAUSS_NOISE_STD. The photon noise follows directly from the brightness of the sources, the detector gain, and the number of images. Since holographic imaging is a complex process it is a priori not clear whether we can estimate the noise in the reconstructed images in the same way as for a standard AO image. Also – and this is also relevant for AO

images – there can exist other sources of uncertainty, like systematic errors in the applied flat-fields or introduced by correlated noise in the readout electronics (often visible in short-exposures, e.g. in the form of horizontal stripes). Also, the signal-to-noise-ratio in mosaicked images will generally not be constant across the image.

Therefore, we explored three different methods to estimate photometric and astrometric uncertainties: (1) *Formal method*: Formal uncertainties evaluated by *StarFinder*, given a noise map composed only of Gaussian plus photon noise. The Gaussian noise was evaluated directly from the image with the GAUSS_NOISE_STD routine. (2) *Sub-map method*: Instead of using a noise map, N independent images are analysed. The uncertainties are estimated from the error of the mean of the stellar positions and fluxes. The independent images, termed *sub-maps*, are created from non-overlapping subsets of the data, with each set containing a fraction of $1/N$ of all frames. (3) *Noise-map method*: The sub-maps (see previous point) are used to create a noise map, in which each pixel set to the error of the mean at its location (i.e., standard deviation divided by $\sqrt{(N)}$). This noise map is then input into *StarFinder*. Note that estimating the noise is itself a process that is subject to uncertainties. Therefore, for a small number of sub-maps, e.g. $N = 3$, the noise map may contain pixels that deviate significantly from the local mean noise. This can pose a problem for the detection of faint stars. Therefore, we recommend $N = 5$ or larger. Alternatively, for $N = 3$ it is good practice to median-smooth the noise map, e.g., with a square box of 3 to 4 pixels width.

A comparison between the three methods is shown in Fig. 3. There is good general agreement between the three methods. The formal method shows hardly any scattering of the uncertainties. However, we expect larger scatter toward fainter magnitudes and also because of other effects, like stellar crowding. Therefore we conclude that the formal method may be helpful for statistical purposes, but may not be helpful to estimate the uncertainties for *individual* stars. If one is interested in the uncertainties of individual targets, use of one of the other two methods is recommended, where the scatter of the errors appears more realistic. Visual inspection reveals that outliers, i.e. stars with uncertainties significantly above the mean for a given magnitude bin, are located close to brighter companions. Since this agrees with our expectations, we take this as evidence that the sub-map and the noise-map methods provide realistic uncertainty estimates.

A disadvantage of the sub-map method is that the sub-maps are less deep than the image reconstructed from all data. Therefore the uncertainties are larger and the detection limit is shallower than in the deep image reconstructed from all data. Also, if the number of sub-maps is small, then the uncertainties tend to be overestimated. Our preferred method is therefore the noise-map method, which allows us to do astrometry and photometry on the deep image reconstructed from all frames. In contrast to the formal method, which tends to lead to the detection of numerous spurious sources in the halos of bright stars, both the sub-map and the noise-map methods lead to robust source detection, as long as a reasonable flux threshold, typically $3\,\sigma$ is applied. The sub-map method has been applied previously to both speckle and AO data (Ghez et al. 2008). We note that the noise-map method appears to be equally robust, but more sensitive to faint sources. It can also be applied to the analysis of normal AO images.

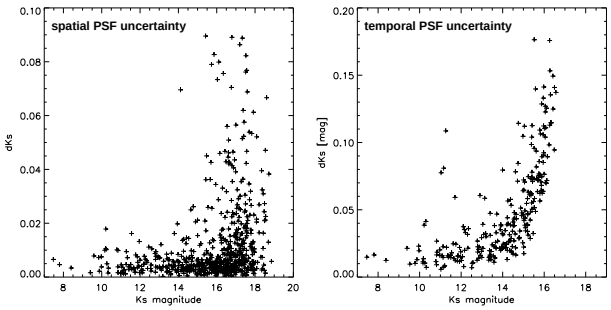

Figure 4. Left: Photometric uncertainties caused by spatial variations of the PSF in the holographic $Ks-$band image of NGC 3603. Right: Photometric uncertainties caused by temporal variations of the PSF for the same data.

3.1.2 Spatial and temporal stability of the PSF

Finally, there is the question of PSF stability. *StarFinder* assumes a perfectly known and spatially stable PSF, which is, of course, an assumption that will always be violated to a certain degree, mainly because of anisoplanatic effects. In order to investigate the effects of spatial variations of the PSF, we performed repeated PSF fitting photometry and astrometry with three different PSFs, estimated from independent sets of reference stars. Note that mean offsets in photometry and astrometry will appear when an image is analyzed with slightly different PSFs. Those mean offsets (on the order of $0.02-0.03$ mag for photometry and $0.001-0.01$ pixels in each axis for astrometry) are not relevant for our analysis and were removed before combining the lists resulting from the different runs of *StarFinder*. Subsequently, uncertainties were estimated from the standard deviation of the measurements with the three different PSFs. The photometric uncertainties are shown in the left panel of Fig. 4. As expected, they appear to be independent of stellar magnitude (the higher scatter at faint magnitudes is mainly due to there being more faint than bright stars) and very low, with a median of 0.008 magnitudes. The astrometric uncertainty, shown in the right panel of Fig. 4, has a median uncertainty of < 0.01 pixels in each axis.

The photometric and astrometric uncertainties from the *temporal* fluctuation of the PSF were estimated by running *StarFinder* on images reconstructed from 10 consecutive data cubes of ∼500 frames each (i.e. total exposure times of the reconstructed images ∼55 s). The uncertainties caused by temporal fluctuations of the PSF were estimated from the standard deviation of the measurements on the ten different images, after correction of the mean offsets (which were somewhat smaller than for the spatial PSF variation). They are shown in the right panel of Fig. 4 and dominate the uncertainties for bright stars. They are $\leqslant 0.02$ mag for stars brighter than $Ks \approx 14$. The corresponding astrometric uncertainties are $\leqslant 0.03$ pixel in each axis for stars brighter than $Ks \approx 14$.

We conclude that the $Ks-$band holographic imaging of the core of NGC 3603 has led to images with a spatially and temporally stable PSF. The photometric uncertainty - using

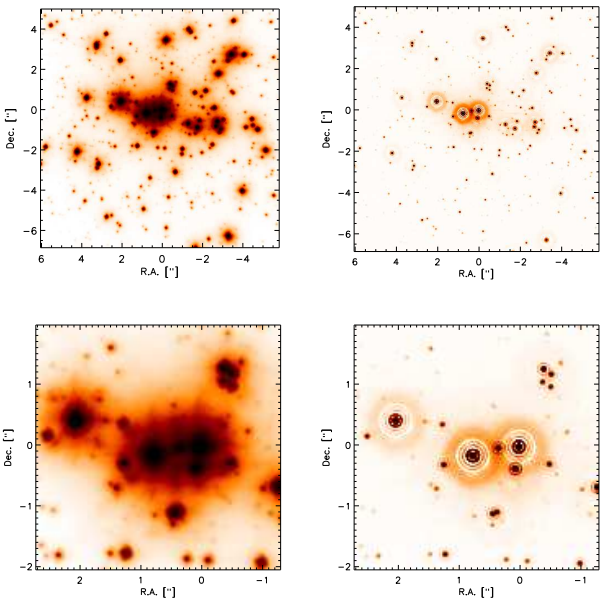

Figure 5. Top left: AO image (Ks-band) of the core of NGC 3603. Top right: Speckle holographic image (Ks-band) of the same FOV. The images on the bottom left and right are zooms into the centers of the two images. Identical logarithmic color scales have been applied to all images.

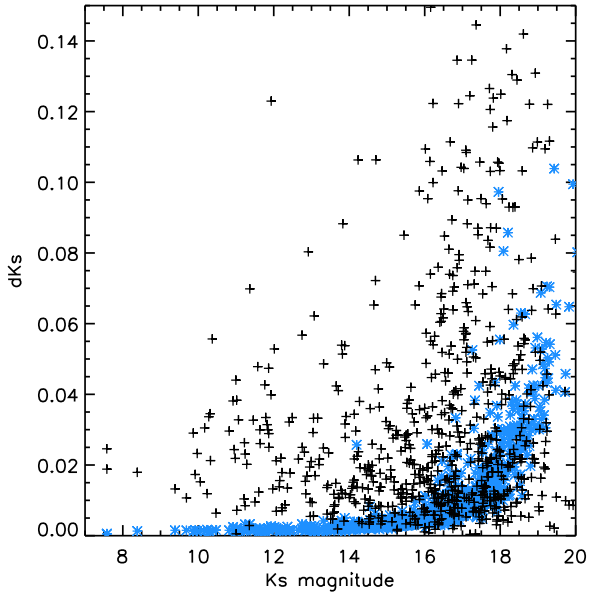

Figure 6. Photometric uncertainties in the AO image. Blue asterisks are the uncertainties estimated from *StarFinder*. assuming a constant PSF. Black crosses are the uncertainties derived from the use of three different PSFs.

the noise map method preferred by us - is $\leqslant 0.01$ mag for $Ks \leqslant 15$ stars. The 3σ detection limit is $Ks \approx 18$, for a total integration time of $4907 \times 0.1\,\mathrm{s} \approx 490\,\mathrm{s}$.

3.1.3 Comparison with AO imaging

Since holography is a non-standard imaging technique, a comparison with a NACO AO image of the same region is of great interest. There are several suitable data sets on the ESO Science Archive. As AO observations with DITs of several seconds seriously saturate the stars in the dense, bright core of NGC 3603, we chose observations with a short DIT. We found two adequate Ks-band observations for our purpose, one from 15 Feb 2005, with DIT= 0.35 s, and one from 20 April 2008, with DIT= 0.5 s. Both data sets are fairly equivalent and we examined both of them. Here we just present the 2008 data set because the seeing was better during the 2008 observations and because the 2005 data set shows a strongly variable PSF over the FOV. The visual seeing during the 2008 observations according was ~ 0.7", i.e. somewhat worse than during the speckle observations. After standard data reduction (sky subtraction, flat-fielding, bad pixel correction) the AO frames were combined with the *eclipse jitter* routine. The total observing time of the AO observations was 1290 s (DIT= 0.5 s, NDIT= 60, N= 43). This is a factor 2.6 longer than for the speckle observations. In Fig. 5 we show the AO and speckle holography images along with close-ups of the central region.

The PSF of the AO observations has a Strehl of $21 \pm 0.02\%$, estimated from three different PSFs created with *StarFinder* using three disjoint sets of reference stars. The $3\,\sigma$ detection limit in the AO image is $Ks \approx 20$. The sensitivity of the AO image is higher than in the speckle image because the speckle imaging data are limited by detector readout noise and, to a lesser degree, because the total integration time of the AO image is significantly longer.

One may argue that the comparison were fairer if we compared the holographic image with a deconvolved and beam restored AO image. However, we refrain from doing so because of the artifacts and possible astrometric and photometric biases introduced by the typical deconvolution techniques, as we have already mentioned in section 3.1.1. It would be ideal to apply holographic image reconstruction to the AO data. However, holographic reconstruction needs a large number of frames (hundreds to thousands) with randomly varying PSF. This is not the case for the available AO data. We will show an application of holography to AO data in section 4.8.

StarFinder was used for photometry and astrometry on the AO image. The noise map method was used, i.e. three images were created from a third of the AO data each; they were then combined to a noise map that was used as input into *StarFinder*. The photometric uncertainties are indicated by the blue asterisks in Fig. 6. The uncertainties rise less steeply toward fainter magnitudes than for the holography image because of the better noise statistics (the AO images are sky-limited, not detector limited). Fig. 6 also shows the uncertainties estimated from photometry with three different PSFs extracted from three different sets of reference stars (the same ones as in the holography image). The uncertainty due to spatial variability of the PSF has a median of 0.02 mag and is larger than in the case of the holography image.

Close stars with great brightness differences can be separated in the speckle image. For example, we reliably identify a star of $Ks \approx 15.8$ at only 0.18" distance from a star with $Ks = 10.0$. As concerns the AO image, the PSF is

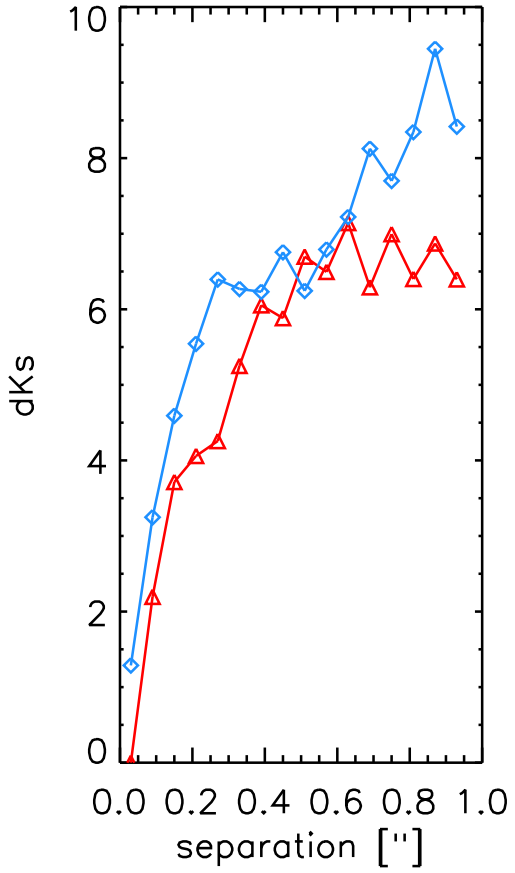

Figure 7. Ks-magnitude difference vs. separation for pairs of detected stars in the AO image (red triangles) and in the holography image (blue diamonds). See text for details.

complex and are numerous spurious sources picked up by *StarFinder* in the wings of the PSFs of bright stars. Detection of spurious sources is far less problematic in the reconstructed speckle image because of the very well defined PSF. Also, contrary to the AO image, the speckle image is not affected by detector non-linearity and saturation of the brightest sources. The total dynamic range of the holographic image is about 11 magnitudes.

As a further test, we compare the angular separation and the magnitude difference for all detected pairs of stars in the AO and speckle holographic images. In order to suppress spurious sources, we ran *StarFinder* with three different PSFs, extracted from three independent sets of stars, on both the AO and holography images. Only stars detected with all three different PSFs and coincident within 0.5 pixels were accepted into the final list. The result is shown in Fig. 7, where we plot the dynamic range vs. separation for all possible pairs of detected stars. This means that one star can appear multiple times in the plot. In order to plot a clear graph that is not too noisy or over-crowded with points, we grouped the detected pairs into bins of 0.06" width (approximately one resolution element with NaCo at Ks). The dynamic range was then taken as the magnitude difference that comprises 90% of all pairs within one bin. As can be seen,

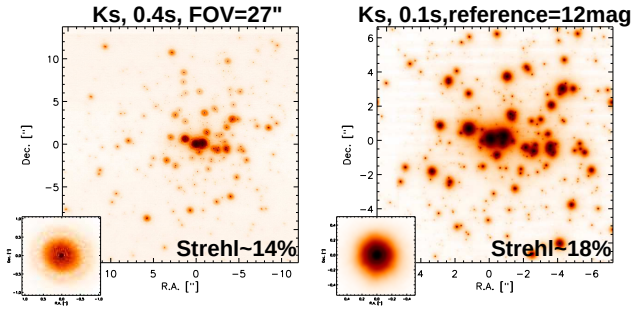

Figure 8. Left: Reconstructed Ks-image of NGC 3603 from speckle imaging with 0.4 s exposure time. Right: Reconstructed Ks-image of NGC 3603 form the observations described in section 3, using only a single reference star of $Ks \approx 12$. The corresponding PSFs are shown in the insets.

at most separations the holography image has a higher dynamic range for the detection of faint companions than the AO image. The peculiar small-scale features of the trends shown in Fig. 7 are probably related with the shapes of the PSFs in both images. We did not investigate this point further.

For an exact quantitative comparison between speckle and AO imaging, the AO and speckle imaging data should be taken under the same atmospheric conditions with the same on-source integration times, of course. Nevertheless, the comparison in this section demonstrates that speckle holography technique as implemented in our algorithm can be highly useful for high-precision astrometry and photometry and for the detection of faint companions in stellar clusters. We show another comparison between holography and AO imaging in section 4.5.

4 FURTHER TESTS OF HOLOGRAPHIC IMAGING

4.1 Faint guide stars

The faintest stars barely visible on individual speckle frames of NGC 3603 (0.1 s exposures) have $Ks \approx 13$. We tested image reconstruction by using a single, isolated star of $Ks = 12$. The reconstructed image and the corresponding PSF are shown in Fig. 8. Very good image cosmetics and a Strehl ratio of $\sim 18\%$ were reached. Using $\sim$8 reference stars with magnitudes $11.5 \geqslant Ks \geqslant 12.5$ improved the Strehl ratio of the reconstructed image to $\sim 22\%$. In the Galactic center data set (section 4.5), we used 24 reference stars of $Ks \approx 13$ and reached a Strehl $\sim$50% in the reconstructed image.

4.2 Long exposure times

Since the short exposure times necessary for speckle imaging require windowing on some detectors (e.g. 512×514 on the NaCo detector for $DIT = 0.1$ s), a question of high interest is whether the speckle imaging technique can also work with exposure times significantly longer than atmospheric coherence time. To test this, we observed NGC 3604 on 3 August 2010 in the Ks-band, using $DIT = 0.4$ s, which allowed us to take advantage of the full NaCo detector FOV. Visual seeing was $\sim$0.6", airmass 1.7 – 1.8. 1125 exposures

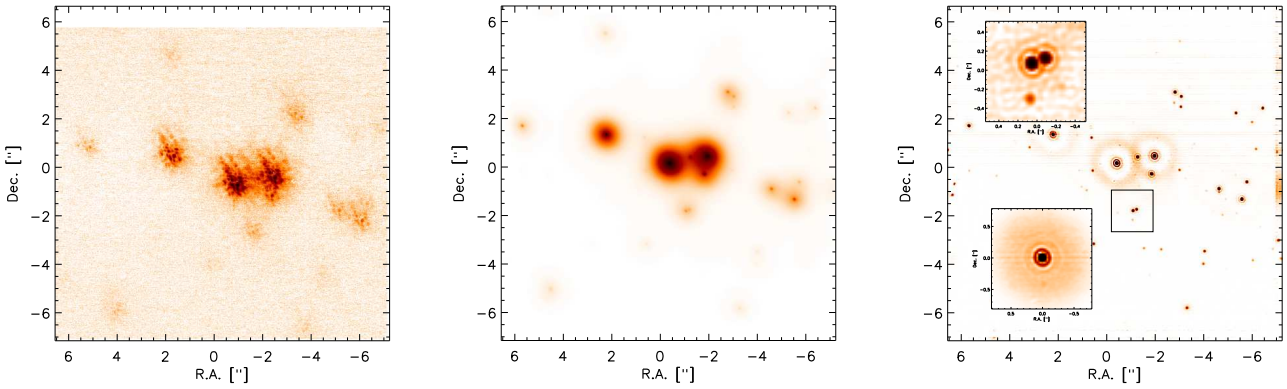

Figure 9. J-band speckle imaging fo the core of NGC 3603. Left: single speckle frame; middle: SSA image; right: image reconstructed with the speckle holography technique. The lower left inset shows the PSF. The upper left inset shows a zoom of the region indicated by the black box. It contains two stars of $\Delta mag \approx 0.5$ that are separated by $\sim$0.08"

of $DIT = 0.4$ s were taken. Holographic image reconstruction was performed by using about 8 relatively isolated stars of $Ks \approx 10$ distributed across the FOV. The reconstructed image and the corresponding PSF are shown in Fig. 8. The diffraction limit was reached with a relatively uniform PSF across the FOV with a Strehl of $\sim$ 13%. Note that anisoplanatic effects are present across the FOV. The Strehl ratio could be improved even more through piecewise reconstruciton of the image, as demonstrated for $I-$band data in section 4.4.

4.3 Short NIR wavelengths: $J-$band

How well does holographic imaging work at shorter wavelengths? The core of NGC 3603 was observed with NACO's *cube mode* on 28 January 2010, using the J-filter, the S13 camera, and with the AO loop open. Visual seeing was $\sim$ 0.5". Windowing was set to 512×514 pixels and the DIT to 0.11 s. Ten cubes of about 500 frames were observed with dithering of a few arcseconds between each series of exposures. Five cubes of a nearby field empty of stars were taken in order to measure the sky background. Standard data reduction steps were applied, i.e. sky subtraction, flat-fielding, and interpolation of bad pixels. In total, 4928 pre-processed speckle images were obtained, corresponding to a total integration time of 542 s.

The three brightest stars at the center of the field were used as reference sources for extraction of the instantaneous PSF from each speckle frame. The instantaneous PSFs were improved by iterative extraction, as described above. A single speckle frame, an SSA image, and the reconstructed image via speckle holography are shown in Fig. 9. Image quality is excellent, the Strehl of the PSF of the reconstructed image is estimated to be 38%. The three reference stars have magnitudes $J \approx 9$. For comparison, the ESO NACO preparation software (*http://www.eso.org/sci/observing/phase2/SMGuidelines/-NAOS.html*) predicts an on-axis Strehl ratio of about 20% under similar atmospheric conditions and with a *visual* guide star of $V = 9$. With an infrared guide star of $J = 9$ the predicted on-axis Strehl is merely about 13%.

4.4 Optical wavelengths: I-band

FASTCAM is an optical speckle camera that is operated as a guest instrument on telescopes such as the 2.5-m Nordic Telescope or the 4.2-m William Herschel Telescope at the Observatorio del Roque de los Muchachos on the Canary Islands (Labadie et al. 2003). Optical speckle imaging has experienced a comeback in recent years. The speckle frames are usually processed via the SSA algorithm, combined with strong frame selection, the so-called *lucky imaging* technique (e.g., Hormuth et al. 2008). Here, we use $I-$band (0.872 μm) observations of the core of the globular cluster M15, obtained with FASTCAM at the 2.5-m NOT, with a pixel scale of 31 mas. 50, 000 individual frames were obtained with an exposure time of 30 mas each.

Frame selection for lucky imaging can be performed in an easy, but effective way, by using the flux in the brightest pixel of the PSF of a reference star. The left panel of Fig 10 shows the SSA reconstruction of the core of M15 after selecting the best $\sim$8.5% of the data. The achieved Strehl is $\sim$2% and the dynamic range between the brightest and faintest detected star is about 6 magnitudes

Visual seeing during the observations was about 1", leading to mediocre data quality, with even the brightest stars being barely visible in many frames. Therefore we had to apply frame selection even for holographic reconstruction. The best 50% of the frames were used. A Strehl of $\sim$7% was reached in the reconstructed image, with a dynamic range of about 8.0 magnitudes.

The Strehl is relatively low in both cases, because isoplanatic effects become more important at shorter wavelengths. In the $I-$band, the isoplanatic angle is only on the order of a few arcseconds, while the FOV of FASTCAM is about 15". To deal with these effects, we divided the FOV into five overlapping subfields of about 9.5" size each. Holographic reconstruction technique applied to these subfields separately, using between 2 and 4 reference stars in each subfield. The final reconstructed image was created by creating a mosaic of the reconstructed subfields. The optimal shifts between them were determined via cross-correlation. Thus, a Strehl of $\sim$18% was reached, with a dynamic range

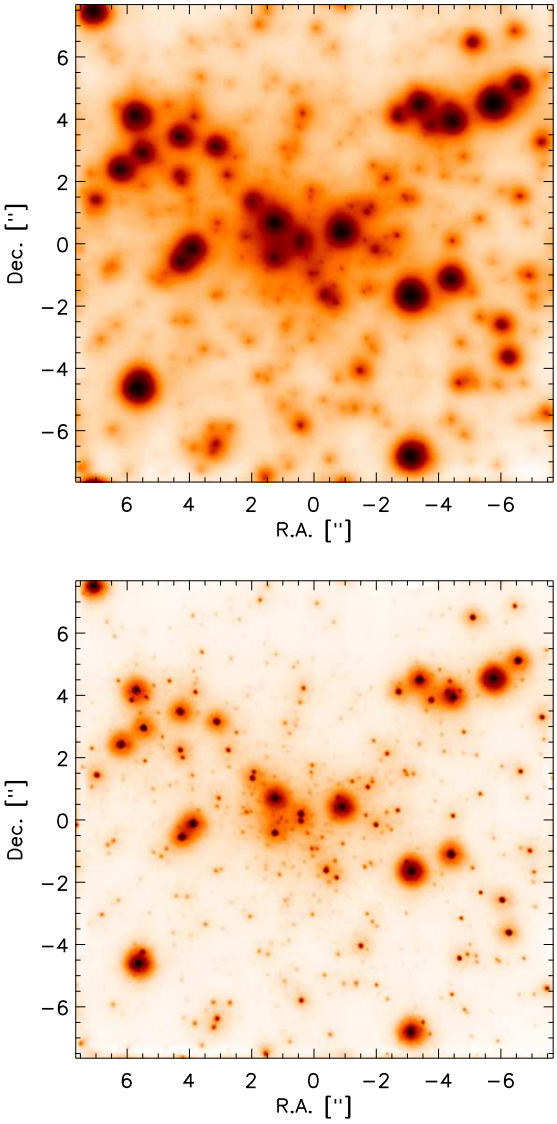

Figure 10. Top: SSA image of optical speckle data of M15 with FASTCAM, after selecting the best ∼8.5% of the frames. Bottom: Holographic reconstruction, using the best ∼50% of the data, and reconstructing five overlapping subfields separately to deal with anisoplanatic effects.

of about 8.5 magnitudes. The corresponding image is shown on the right panel of Fig. 10.

4.5 $K-$band imaging of the Galactic center with NaCo/VLT

The Galactic centre (GC) provides a highly interesting test case because of the extreme stellar crowding around the supermassive black hole Sagittarius A* (Sgr A*). It is a prime target for high resolution imaging and precision astrometry. Both speckle and AO imaging have been used since the early 1990s to measure the proper motions of stars in the vicinity of Sgr A* and, in fact, to infer its very nature (e.g., Eckart & Genzel 1996; Ghez et al. 1998, 2003; Schödel et al. 2003; Gillessen et al. 2009).

The GC was observed with NaCo/VLT in burst mode on 7 August 2011, acquiring ∼12.500 frames of exposure time 0.15s through the Ks-filter. Visual seeing varied between ∼0.6" − 0.9" and the atmospheric coherence time was $\tau_0 \approx 2$ ms, i.e. seeing was fast. Detector windowing was set to 512×514 pixels. Sky exposures were obtained on an empty field in a dark cloud a few arcminutes offset from Sgr A*. Reduction of the short exposures followed the standard procedure for NIR imaging.

Holographic imaging provides excellent results on these data and we here describe several key tests of our algorithm:

- Performance in this extremely crowded field is highly satisfactory. Using 10 reference stars of $Ks = 7.5 - 11$, distributed across the field, an image with a final Strehl > 80% and excellent PSF cosmetics has been reconstructed (Fig. 11, panels (a) and (b)). The $3\,\sigma$ detection limit is $Ks \geqslant 19$ in 1875 s of total integration time. The achieved dynamical range is about 12 magnitudes.
- Holography with multiple, faint reference stars provides excellent results. Using 24 stars of $Ks = 13 \pm 0.5$, a Strehl ratio of 45% was reached in the reconstructed image (Fig. 11, panel (c)). Such a feat is beyond the capabilities of any existing AO system, to the best of our knowledge. Since the Galactic centre region contains a high density of $K \leqslant 12$ stars, usually more than one per isoplanatic angle in the K-band (Schödel et al. 2007), the holography technique can free us thus of the restrictions imposed by the need for bright reference stars of single conjugated AO systems and the problems related to LGS-supported AO imaging (cone effect, need for tip-tilt) reference star. The large density of reference stars can allow us further to compensate for anisoplanatic effects and create images with great PSF stability. This applies not only to the GC, but also to other dense clusters, particularly highly extincted ones. We do in no way want to discredit AO (almost all authors of this work are avid users of AO systems and the superiority of AO in some aspects is shown further below), but show that there are situations where another approach can reach superior results.
- Contrary to AO with natural guide stars, holographic imaging of a dense cluster allows the observer to adjust the center of optimal correction. As an illustration, we reconstructed the image just using the brightest star in the field, IRS 7, as reference source. Since IRS 7 is located approximately 5.5" north of Sgr A*, the correction is not optimal in the environment of the black hole (Fig. 11, panel (d)).
- Reconstruction of extended sources, like the well-known bow-shock star IRS 1W, provides no difficulties (Fig. 11, small black rectangle and inset into panel (a)).

We compared the holographic image of the GC with a $Ks-$band AO image of the same region. AO assisted imaging observations fo the GC have been performed with NaCo on a regular basis since 2002. The quality of the AO image chosen here is exceptionally high. The observations were taken on 31 March 2009 with visual seeing 0.4" − 0.5" and coherence time of ∼47 ms. The exposure time was set to 1.0 s and the total integration time of the data is 1920 s. The loop of the AO was closed on the supergiant IRS 7, located ∼5.5" north of Sgr A*, the brightest star visible in the image shown in the panel (a) of Fig. 11.

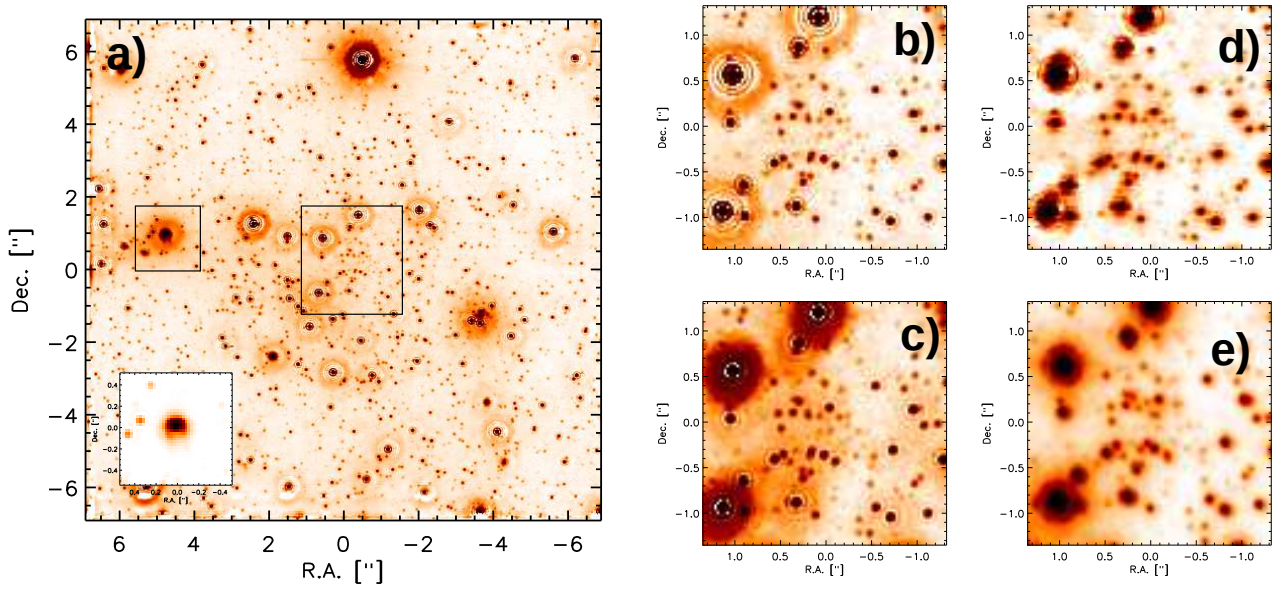

Figure 11. Holographic imaging of the Galactic center with NaCo/VLT, $Ks-$band. (a) Image reconstructed with about 10 reference stars of $Ks \approx 7-11$. The rectangles mark the center field shown in panels (b), (c), and (e), and the source IRS 1W shown in panel (d). (b) Close-up of the environment of Sgr A*. (c) Like (b), but from an image reconstructed with the use of 24 $Ks \approx 13$ stars. (d) Like (b), but from an image reconstructed with only one reference star, the $Ks \approx 7.5$ IRS 7, the brightest star in the field shown in (a). (e) Close-up of IRS 1W from panel (a).

As a side remark, note that the magnitude of IRS 7 is usually cited as $Ks \approx 6.5$ (Blum et al. 1996). However, Ott et al. (1999) showed that IRS 7 is variable, with its magnitude decreasing throughout the time interval examined by them (1992 to 1998). IRS 7 is saturated on almost all AO observations and reports on its magnitude are rare. It is not saturated in our speckle observations and we determined its magnitude to $Ks = 7.50 \pm 0.03$ for August 2011, i.e. a magnitude fainter than what is usually cited. This agrees with the $Ks = 7.69 \pm 0.06$ reported for April 2006 (Schödel et al. 2010). For the AO data analysed here we find $Ks = 6.96 \pm 0.04$ (after repairing its saturated core with *StarFinder*), showing that it was almost 0.5 mag brighter in this epoch, which will have resulted in improved AO performance compared to other epochs. The environment of Sgr A* as seen in the AO image is shown in Fig. 11, panel (e). Note that some of the stars near Sgr A* have moved because the holography and AO epochs lie 2 years apart.

A quantitative comparison of PSF fitting photometry in the AO and in the holography images is shown in Fig. 12. The analysis was done on the FOV shown in panel (a) of Fig. 11. The detection threshold of *StarFinder* was set to $5\,\sigma$ and the correlation threshold to 0.9 in order to suppress the detection of spurious sources. The AO image is about 2 mag deeper than the holography image. Also, the dynamic range for detection of close stellar pairs is 1 to 2 magnitudes higher in the AO image. On the other hand, the photometric uncertainty for stars $Ks \leqslant 14$ in the holography image is smaller than in the AO image. It has to be kept in mind that seeing was significantly better for the AO observations. In particular, the coherence time was a factor > 10 longer than for the speckle observations. So, while the comparison

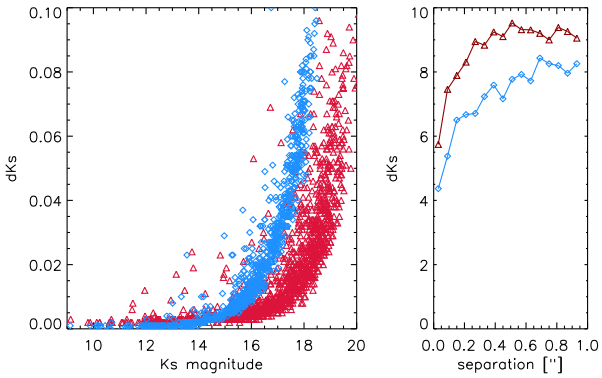

Figure 12. Quantitative comparison of the photometry in the holographic (7 August 2011) and AO (31 March 2009) $Ks-$band images of the Galactic center with NaCo/VLT. Left panel: Measured uncertainty vs. magnitude. Right panel: Dynamic range vs. separation for stellar pairs (see also Fig. 7 and description in section 3.1.3. Blue diamonds for holography and red triangles for AO data.

with AO imaging in the case of NGC 3603 (section 3.1.3) probably favoured holography, the comparison here favours AO.

4.6 $K-$band imaging of the Galactic center with Keck/NIRC

Between 1995 and 2005 the Galactic center was observed with the speckle camera NIRC at the Keck telescope in

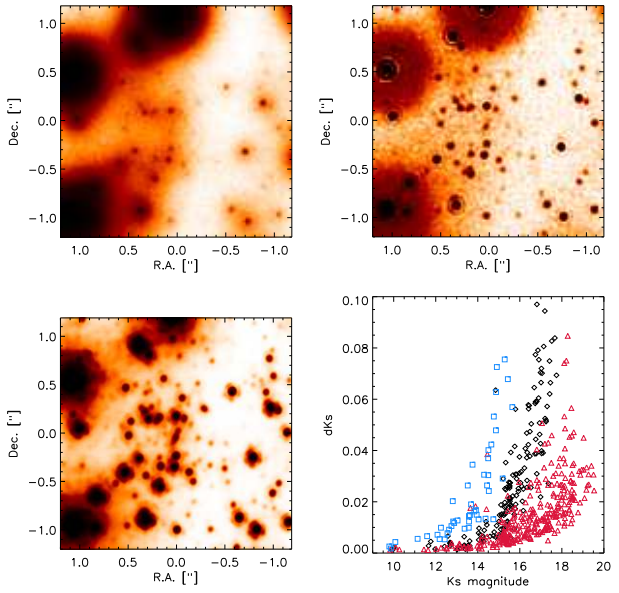

Figure 13. Speckle holography of the Galactic center with NIRC/Keck. Upper left: SSA image of the central arcseconds of the Galactic center NIRC/Keck from April 2005. Upper right: Image reconstructed with the holography technique. Lower left: NIRC2/Keck LGS AO image of the Galactic center from July 2005. Lower right: Photometric uncertainty vs. K-magnitude for sources detected within 2" of Sgr A*s: blue squares: SSA; black diamonds: holography; red triangles: AO.

order to monitor the motion of stars around Sgr A* (e.g. Ghez et al. 2008). We have applied our holographic image reconstruction method to these data. They are of special interest because the holographic technique allows us to detect fainter sources than in the previously used SSA images. Thus, it becomes possible to track the orbital motion of stars that are too faint to have been picked up in the previously used SSA images. Also, crowding can lead to systematic errors in the measured positions of the stars close to Sagittarius A* (see Ghez et al. 2008; Gillessen et al. 2009). The excellent Strehl ratio of the holographic images enable us to disentangle close sources with a large dynamic range. Since the methodology presented in this paper was in large parts developed and fine-tuned with NIRC speckle data of the GC and since the holographically reconstructed GC data will be used in future publications, this work is the natural place to explain the corresponding details.

As an example, we present a data set from April 2005. About 10,000 speckle frames with an exposure time of 0.1 s were used for image reconstruction. The stars IRS 16C, IRS 16NW, and IRS 16SW were used as reference stars ($Ks = 9.9$, $Ks = 10.1$, and $Ks \approx 10.2$, see Schödel et al. 2010).

A special feature of the NIRC GC speckle data is that they were collected in the so-called *stationary mode*, which keeps the pupil fixed on the detector. This avoids a variable contribution of the secondary spider to the diffraction patterns. A part of the FOV was masked in all NIRC data, with the mask changing relative to the stars because of the sky rotation. In order to deal with the variable FOV, we constructed a weight map to adjust the final reconstructed image. The weight map was created by running the corresponding masks of all the speckle frames through the same holographic reduction pipeline. We used an airy PSF for a circular 10m-aperture for apoisation of the final image. The FWHM of this airy function, ∼0.05", corresponding to the anguler size of a resolution element of the Keck telescopes in the $K-$band.

In Fig. 13 we show close-ups on the environment of Sagittarius A* from an SSA and a holography image for the April 2005 data, as well as from a laser guide star (LGS) assisted AO image from July 2005 (Ghez et al. 2008). A plot of photometric uncertainty vs. magnitude for the point sources detected in the three images is shown in the same Figure. Lucky imaging was applied to the SSA reconstruction, with selection of the best 10% of the frames. The exposure times of the AO (∼900 s) and holography (∼1000 s) images are comparable. As can be seen in Fig. 13, holographic image reconstruction provides excellent spatial resolution with a very well calibrated PSF in the reconstructed image. The sensitivity in the AO image is, of course, significantly higher because of the longer frame integration times. The holography image is roughly 2 magnitudes deeper than the SSA image, while the AO image is about 2 magnitudes deeper than the holography image.

4.7 MIR wavelengths, reference sources with extended emission

Because of the short readout times necessary in mid-infrared (MIR) imaging, speckle techniques are naturally suited to improve images at these wavelengths. The MIR imager and spectrograph VISIR at the ESO VLT can save individual exposures in the so-called *burst mode* (see Doucet et al. 2006). WE have applied the holography technique to VISIR 8.6 μm-imaging data of the Galactic center, as described in Schödel et al. (2011). The ∼5 Jy source IRS 3 was used as reference source. It was thus possible to reconstruct fully diffraction limited (FWHM≈ 0.25"), high-Strehl ($\geqslant$ 90%) images of the Galactic center, even during visual seeing as bad as $\sim 2-3$". A seeing of 2" corresponds to an uncorrected point source FWHM of ∼1" at 8.6 μm, according to the Roddier formula.

A particular feature of the described MIR data is that the reference source, IRS 3, sits atop extended, diffuse emission (e.g., Pott et al. 2008, , their Fig. 1). The PSF extraction algorithm was modified to deal with this situation in the following way. First, the background and noise of the PSF were estimated as described in section 3. Then, a constant value of the background plus 5σ times the noise were subtracted from all pixels of the preliminary PSF estimates. All values that were subsequently < 0 were set to zero. In this way, the extended emission is always below the threshold in each frame, and will not contribute to the estimates of the instantaneous PSFs. Systematic uncertainties caused by the extended emission are thus avoided. This approach lies intermediate between holography, that uses the entire instantaneous PSFs for image reconstruction, and weighted shift-and-add, that uses the relatively weighted peaks of the instantaneous PSFs (Christou et al. 1987).

We conclude that holography is naturally suited for MIR imaging and can serve to achieve optimal image qual-

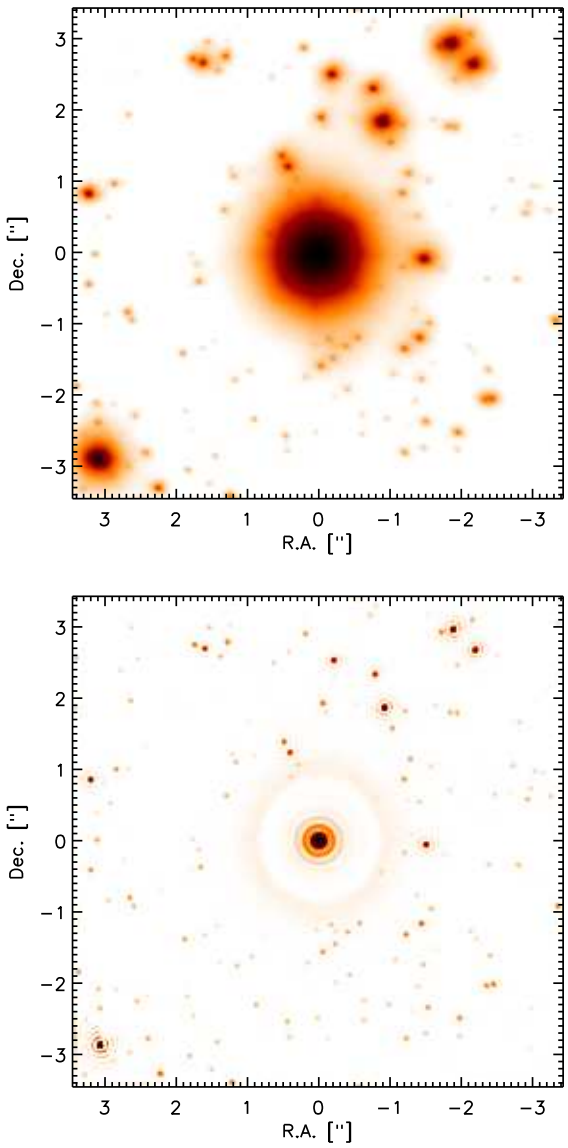

Figure 14. Top: SSA combination of ∼1900 3 s-exposures of a field centered on the star 2MASS 00241142-7205556. Bottom: Holographic image reconstruction, using the same data set.

ity even under the most adverse seeing conditions, given the availability of (a) suitable reference source(s). Since the technique will also work for point sources that lie atop extended emission, this provides new possibilities for MIR imaging of sources like AGN or planetary nebulae. In both technical and image reconstruction aspects, holography is less complex than sparse aperture masking and may provide greater sensitivity because it is not necessary to block a large percentage of the light.

4.8 Holography plus AO

A disadvantage of holographic imaging are the necessarily short exposure times. This limits severely the sensitivity to faint sources because the data are dominated by detector readout noise. Longer exposure times become possible with the help of AO. However, this will only be useful if the AO PSF is *not completely* stable, i.e. if the PSF shows some random variability on time scales similar to the exposure time. In that case, the holography technique can help to suppress the random fluctuations through averaging over a large numbers of frames (see Equ. 1). For example, under bad seeing conditions or at short wavelengths, the AO loop may not work perfectly. In fact, the cube mode of the NaCo instrument was originally implemented to enable frame selection, i.e. *lucky imaging*, which is useful at short wavelengths (e.g., Kervella et al. 2009). As in standard lucky imaging, AO assisted lucky imaging will discard a significant amount of flux and information and could profit from the application of holographic image reconstruction.

We have tested this *holography plus AO* technique on Ks imaging data obtained with NaCo on a field in the globular cluster M15. Seeing in the visual was on the order of 1", but the coherence time was just a few milli-seconds and AO correction was not stable: Although the exposure time was as long as 3 s, the PSF is clearly variable between the frames. In Figure 14 we show a comparison between a SSA combination of the ∼1900 frames from this data set and a holographic image reconstruction from the same set of frames. The AO guide star ($V \approx 13, Ks \approx 9.7$) was used as reference source. Application of holographic reconstruction improves the resolution of the image, without the strong ringing of Wiener devonvolution or the grainy background of Lucy-Richardson deconvolution. The isoplanatic angle was extremely small, on the order of just a few arcseconds in the Ks-band. Therefore, we only show a small field.

Hence, similar as the performance of sparse aperture masking can be boosted by the stabilising effects of AO, speckle holography can also be booster by AO. There is, however, one catch: If the exposure times are larger than the tip-tilt timescale, then isoplanatic effects may become frozen into the images. That is, the ability of holography to deal with anisoplanatic effects may be lost when combining it with AO.

4.9 Large FOVs, improved sensitivity: Under-sampling the diffraction limit

Deliberately under-sampling the diffraction limit appears at first as a bad idea because of the corresponding loss of information. When the condition of Nyquist sampling is not fulfilled, the appearance of the speckle clouds of different stars will depend on the relative pixel positions of the stars. When using multiple reference guide stars, however, some of the information about the PSF can be recovered by image re-sampling and median superposition of the stellar images with sub-pixel accuracy. But even with a single reference star, the systematic errors made on individual frames will tend to cancel each other out for a large number of frames. While reconstruction of an image at the diffraction limit will be difficult (but probably not impossible, if sampling is close to the diffraction limit), it may be possible to achieve a reconstructed image with an angular resolution that is significantly superior to the one imposed by atmospheric seeing. We tested this assumption by simulations.

In order to set up our simulations, we used a NACO Ks-image of a field in the Milky Way nuclear star cluster,

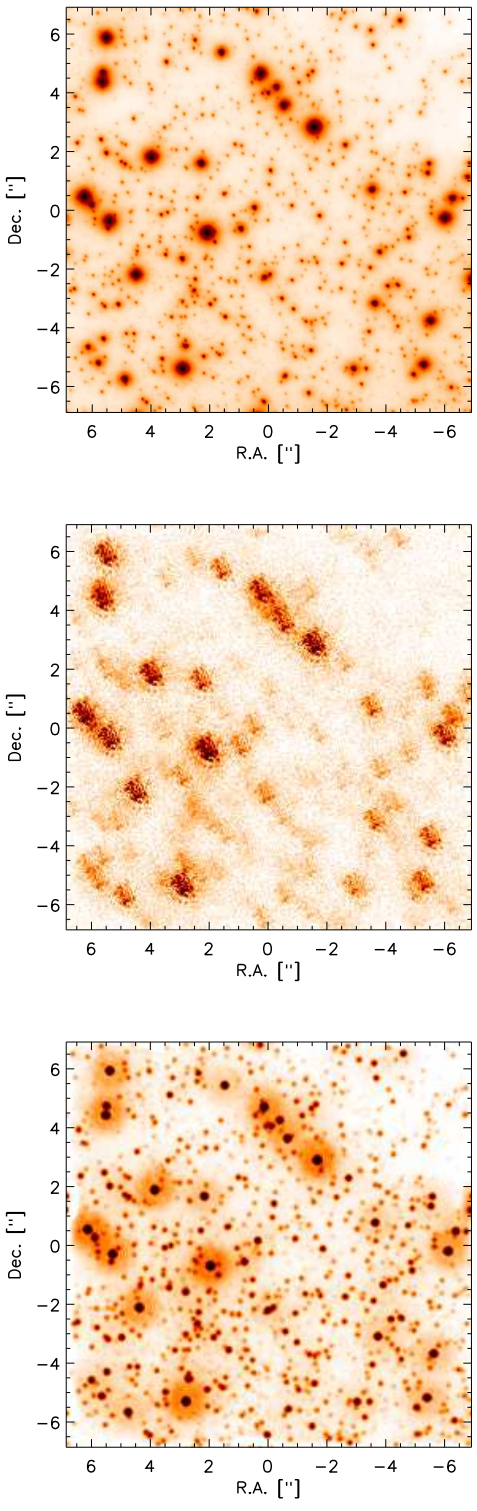

Figure 15. Top: NACO Ks-band AO image of a field in the Milky Way nuclear star cluster roughly 30" north-east of Sagittarius A*. Middle: Simulated speckle frame of the same field, assuming the NACO detector characteristics, the NACO S54 camera, seeing in the visual of 0.8", and $DIT = 0.4$ s. Bottom: Image reconstructed from the simulated speckle observations. The FWHM of the Gaussian PSF is 0.135".

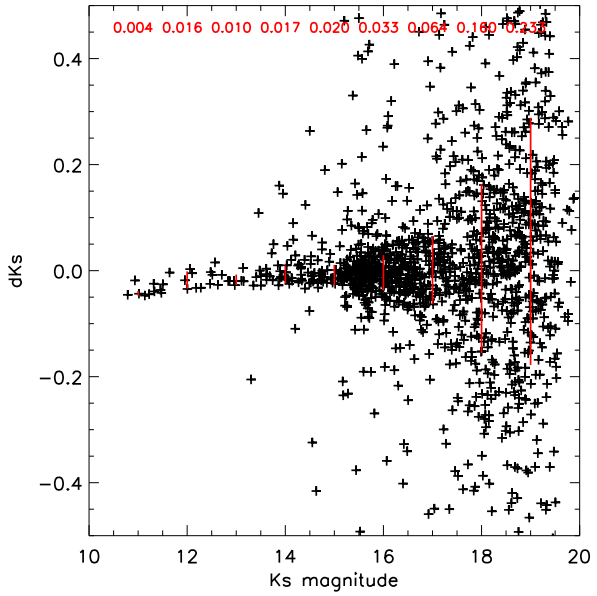

Figure 16. Comparison between input and recovered magnitudes of the stars in the simulations shown in Fig. 15. The red bars and the numbers in red at the top of the graph indicate the standard deviation of the photometric error in bins of one magnitude width.

about 30" north-east of Sagittarius A*, taken on 28 May 2008 (see Schödel et al. 2009). We only used a 14" × 14" sub-field of the observations in order to keep the computing time of our simulations within practical limits. The original NACO AO image is shown in the top panel of Fig. 15. We extracted the positions and magnitudes of the stars measured in this diffraction limited image ($FWHM \approx 60$ mas) to create simulated observations.

We assumed use of the NACO S54 camera, which has a pixel scale of 0.054" per pixel. We further assumed the gain and readout-noise of the NACO detector (see ESO manual) and use of the Ks-filter. The integration time of individual frames was set to 0.4s, seeing in the visual to 0.8″, and the wind speed to 10 m/s. We simulated 10000 speckle frames, with the corresponding random read-out and photon noise added. A single speckle frame is shown in the middle panel of Fig. 15. The speckle clouds were simulated with the code by Rengaswamy et al. (2010).

A Gaussian PSF of FWHM 0.135" was used as apodization function in the holographic image reconstruction. The resulting image is shown in the bottom panel of Fig. 15 and has a point-source FWHM of 0.135". That is a factor ∼4.5 better than the FWHM of ∼0.6" imposed by atmospheric seeing (using the Roddier formula to evaluate the seeing in the $Ks-$band). A comparison between the input and recovered magnitudes of stars in the simulated image is shown in Fig. 16. The mean photometric uncertainty was calculated from sigma-clipped (to remove outliers) values in bins of one magnitude. The mean photometric uncertainty of $Ks = 16(13)$ stars is a mere 0.03(0.01) magnitudes. The $3\,\sigma$ detection limit is as low as $Ks = 20$.

We conclude that holographic imaging can also be used successfully when the telescope diffraction limit is not Nyquist sampled. In this case holography can serve to obtain

images with a point-source FWHM far superior to the one imposed by atmospheric seeing. Under-sampling the diffraction limit in a speckle camera can have multiple advantages:

- Large field-of-view. For example, use of the NaCo/VLT S54 camera enables one to image a field as large as 56" × 56" with a FWHM on the order of 0.13".
- Increased sensitivity to faint sources. This has the double advantage of being able to detect stars $Ks > 20$ and to use faint reference stars. As we have shown in section 4.5 $Ks = 13$ stars work well with NaCo/VLT. This means that for under-sampled instruments, stars as faint as $Ks = 15$ may serve for satisfactory image reconstruction, depending on the pixel size.
- Use of the holographic technique with already existing instruments. For example, HAWK-I/VLT can be used to achieve images with resolutions of ∼0.25" and a FOV of several square arc-minutes (the exact field is imposed by detector windowing, which is a function of the readout time, e.g., 450" × 70" with 0.2 s exposure time and 450" × 140" with 0.4 s exposure time).

Under-sampling of the diffraction limit is an interesting option to trade off spatial resolution versus increased FOV and higher sensitivity in optical and near-infrared observations (at MIR wavelengths, coarse pixel-scales may actually decrease sensitivity). Many science targets, like the Galactic center, star forming regions, or globular clusters present a sufficient density of bright enough reference stars to actually exploit FOVs of the order one to a few minutes of arc. Wide-field, high angular resolution imaging of these targets can thus be done without the need to build expensive multi-conjugate (or multi-object) adaptive optics systems. Possibly, the increased sensitivity and FOV offered by under-sampling of the diffraction limit can even make holography an interesting technique for some extragalactic observations.

5 DISCUSSION

In the sections above we have demonstrated the excellent performance of our methodology for holographic imaging of dense stellar clusters. In this section we briefly discuss the advantages and disadvantages of speckle holography in given observing situations particularly with respect to the alternatives like AO assisted imaging or sparse aperture masking.

5.1 Sensitivity

The most fundamental constrain on holographic imaging is certainly its limited sensitivity. The necessarily short integration times result in detector readout noise dominating the noise budget. Whenever the science targets are faint (e.g., $Ks \geqslant 19$) the long integration times afforded by AO systems are needed. This is the case for almost all extragalactic applications, with the possible exceptions of the close surroundings of bright AGN. An interesting special application for holography would be AGN too faint for the NIR wavefront sensor of NACO and with no suitable tip-tilt star for LGS AO nearby.

However, the constraints on sensitivity are not severe: In just ∼1900 s of total integration time, we have reached a $3\,\sigma$ point-source sensitivity of $Ks \approx 19.5$ in observations of the Galactic center with the S27 camera of NaCo/VLT. This means that the technique is well suited to study star clusters in the Milky Way. With this sensitivity, main sequence stars of G-type can be detected out to 10 kpc, or pre-main sequence stars at the H-burning limit and with an age $< 10^7$ yr can be detected out to ∼3 kpc.

The sensitivity of holographic imaging is clearly superior to sparse aperture masking, even if the latter is supported by AO. The cause is simply that the aperture masks block on the order of 90% of the light.

There are several ways to improve sensitivity. First, detectors and readout electronics can be optimised for short exposure times. For example, the group of G. Weigelt (MPIfR, Bonn, Germany) have reached a readout noise on the order of $10e^-$ in their speckle camera, using a HAWAII-1 detector (priv. comm., G. Weigelt). NaCo uses the same detector type, but has a readout noise that is almost 4 times higher (for the fast readout modes required for speckle imaging). We conclude that sensitivity can be increased by almost 1 magnitude with electronics and readout procedures that are optimised for speckle imaging. Hence, a $3\,\sigma$ point-source sensitivity of $Ks \approx 20$ in 1 h of integration time appears to be an easily achievable goal for speckle holography at the diffraction limit of 8-10m class telescopes with existing technology.

As we show in section 4.9, under-sampling of the diffraction limit is another, rather easy, way to improve sensitivity because it allows to gather more photons per detector pixel. Under-sampling the diffraction limit by a factor of ∼3 (corresponding to a resolution ∼0.18" at an 8m-class or ∼0.05" at a 30m-class telescope in the K-band) would increase sensitivity by more than one magnitude.

Finally, breakthroughs in detector technology are under way in the form of new high speed low noise detector arrays that are being developed mainly for their application in wavefront sensors. While the readout noise of the detector in NaCo, for example, is $44e^-$ rms, read noise $< 7\,e^-$ rms has already been reached in a new detector model (Finger et al. 2010), equivalent to one magnitude gain in sensitivity. Hence, a sensitivity limit of $Ks \approx 21$ at the diffraction limit appears to be easily achievable with the next generation of NIR detectors. Saturation will hardly be a problem with the speckle technique if the stars in the FOV are fainter than $Ks \approx 6$. Hence, the technique can deliver a dynamic range on the order of 15 or more magnitudes.

5.2 Reference stars

AO systems need relatively bright guide stars. For example, NaCo operates with visual guide stars in the range $V \sim 10-16$. This need for a bright guide stars in combination with anisoplanatic effects limits the sky coverage of classical AO systems. Significant improvement, can be achieved with laser guide stars or by using NIR wavefront sensors (currently only NaCo is equipped with a NIR wavefront sensor, which allows its AO to work with $Ks \sim 6-13$ stars).

Here, we have shown that holographic image reconstruction can achieve high Strehl ratios even with relatively faint stars $Ks \approx 13$. A particular advantage of holography is that several guide stars within the FOV can be combined to achieve greater S/N on the instantaneous PSF. Moreover, it is sufficient, if the stars are bright in the NIR, i.e. holography

is naturally suited to investigate highly extincted targets, like the Galactic center, that may even be challenging for LGS observations because of a lack of optically sufficiently bright tip-tilt stars. Following the reasoning of the previous paragraph, optimized electronics and/or detectors can push the brightness limit of the reference stars easily down to by one to two magnitudes. Speckle holography is thus well suited to take a look into the most obscured places of the Galaxy.

5.3 Anisoplanatic effects

Some of the greatest obstacles for AO imaging are caused by anisoplanatic effects. While the instantaneous PSF in a short-exposure image will also be dependent on the line-of-sight, image reconstruction a posteriori provides the great advantage that these effects can be compensated. Sub-fields smaller than the isoplanatic angle can be reconstructed separately and then be re-mosaicked into the final reconstructed image. All that is needed is a sufficient density of reference stars in all parts of the field. We demonstrate the feasibility of this technique in section 4.4. We believe that the method can be refined, for example by using interpolation or principal component decomposition to determine the instantaneous PSF at any location in the field if the reference stars are widely spaced apart. This is, however, beyond the scope of this work. Here we just note that speckle holography (or even simpler image reconstruction methods, like SSA) allows one to deal with anisoplanatic effects. As discussed above, the reference stars can be relatively faint and multiple reference stars within an isoplanatic angle can be superposed. Thus, holography is ideal for imaging large fields in Galactic targets such as young clusters, the bulge, the Galactic center, or globular clusters.

5.4 PSF calibration

As we have shown, speckle holography leads to a well-calibrated PSF with good cosmetics. This can lead to a very high precision in the photometry and astrometry of bright stars, where readout noise is not the dominant source of uncertainty. Holography may thus be well-suited to investigate diffuse structures and faint secondary sources near bright stars. An necessary condition is, however, the presence of either an isolated bright star near the science target or, alternatively, that the science target is embedded in a star cluster. For bright, isolated science targets, AO assisted sparse aperture masking is the preferable technique because of the lack of a nearby PSF calibrator. If the target is isolated, modified holography (i.e. the weighted shift-and-add approach mentioned in section 4.7) can be applied to recover faint stars or diffuse emission.

Modern telescopes are highly adaptive and are conceived with many control loops (active optics, adaptive optics, etc.) which can limit the performance of techniques that require fast switching between science target and calibrator (e.g., sparse aperture masking). For such techniques, it is very important that the telescope optical transfer function stays constant during the entire observation. This is rather difficult to guarantee with a VLT-like (thin mirror) telescope and will probably be nearly impossible with the next generation of extremely large telescopes. Because of the possibility of *self-calibration* speckle holography may thus remain an attractive technique even with the next generation of telescopes and AO systems.

We have shown that speckle holography can reach Strehl ratios that are more than competitive with current AO systems. Holography has the additional advantage that one is free to choose one or several reference stars a posteriori and can thus even choose where to set the center of correction (see discussion in section 4.5 and panels (b) and (c) vs. panel (d) in Fig. 11) and thus optimize correction near the science target.

5.5 Short wavelengths

Our experiments show that, at short near-infrared to optical wavelengths, speckle holography out-competes probably most, if not all, currently existing AO systems. It is also more efficient than lucky imaging because it uses the information and flux in the entire instantaneous PSFs. This capability leads also to a strongly reduced need for frame selection, which additionally boosts sensitivity.

5.6 Specialized techniques

Holography is a technique that is optimal for imaging, but is difficult to combine with additional techniques. It is possible to combine speckle imaging with spectroscopy (see, e.g., Genzel et al. 1997). However, extracting a spectrally dispersed instantaneous PSF is challenging and the spectral dispersion leads to an even lower S/N in speckle frames than in imaging. Therefore, for spectroscopy, use of an AO system is clearly the superior technique. A technique like coronagraphy, or any other technique that requires a temporally stable PSF when the light enters the instrument, cannot be combined with holography. AO is without alternative for such special applications. Since a speckle camera can be built with a very small number of mirrors, the technique appears to be well suited for polarimetry.

An interesting question is when to use AO assisted sparse aperture masking (see Tuthill et al. 2006) and when speckle imaging. In fact, the techniques appear highly complementary. A good examples the science case of detecting stellar companions. Under optimal conditions sparse aperture masking can provide a dynamic range of ∼500, or about 6.7 magnitudes, at angular separations $\theta = \lambda/D$, where λ is the observing wavelength and D is the telescope diameter. At the VLT in the $K-band$ $\theta \approx 0.03$". Sparse aperture masking is optimised to investigate structures on sizes a few times the diffraction limit. In the deep Ks holography image of the Galactic center, presented in section 4.5, we reach a dynamic ranges for companion detection of about 4, 5, 8, and 10 magnitudes at angular separations of 0.06", 0.1", 0.2", and > 0.8". This means that holography can ideally complement sparse aperture masking when investigating multiplicity in stellar clusters.

5.7 Speckle holography and AO

AO systems have undergone tremendous improvements over the past decade and are essential to the success of major ground-based telescopes. They are necessary for high-

resolution, high sensitivity imaging and, in particular, for spectroscopy. Speckle holography can be no replacement for an AO system. However, there are important niches for speckle holography. Since it should always be our aim to optimize resources, particularly in a time where those are scarce, we believe it important to point out that there are numerous situations where speckle imaging can provide a more effective, and more cost efficient, solution than AO. Such niches are, for example, imaging of dense Galactic targets, like starbursts clusters or globular clusters, at short NIR to optical wavelengths. Another attractive application of speckle holography is the imaging of fields much larger than the isoplanatic angel in the Galactic bulge or in the Galactic center. Since holographic reconstruction works with faint guide stars and since its FOV is, in principle, only limited by the detector size (and the ability to read the detector with sufficient speed), holography can serve to image fields of several square arc-minutes size near the diffraction limit of large telescopes. Doing this with AO would require extremely complex MCAO systems with multiple lasers. Because of its simplicity and robustness as well as the unique advantages of a posteriori image reconstruction, holography can also be a very attractive solution for high-angular resolution imaging at short infrared or optical wavelengths with the next generation of extremely large telescopes.

AO and holography do by no means need to be mutually exclusive. A very interesting perspective is to combine the virtues of AO and holographic image reconstruction. Such an approach can be highly advantages in situations when the AO system can only partially stabilize the PSF, for example when it operates at short wavelengths or under very unstable seeing conditions. We have provided a demonstration of the latter application in section 4.8.

5.8 Costs and effectiveness

The probably greatest strengths of a speckle imaging system are arguably costs, robustness, and reliability. Apart from requiring a fast readout, low noise detector and electronics, all other parts of a speckle camera are fairly standard. No complex systems are needed, which are expensive, and require long development and debugging times. The simplicity of a speckle system also means that it is highly reliable and will work under a broad range of circumstances. Additionally, a speckle camera will be of low weight and thus pose no strain for any telescope infrastructure.

6 SUMMARY

An optimized method is presented for applying holographic reconstruction to speckle imaging data of dense stellar fields. The two key features of our methodology are an iterative improvement of the instantaneous PSFs extracted from each speckle frame and the (optional) use of several reference stars simultaneously. The method has been tested with great success on a range of different instruments, wavelengths and targets. Excellent PSF cosmetics and high Strehl ratios have been reached, that can easily compete with existing AO systems. At short NIR to optical wavelengths, the method can outperform currently available AO systems. In dense stellar fields, holographic imaging can deal successfully with anisoplanatic effects and leads to spatially and temporally stable PSFs in the reconstructed images. Holography is superior to lucky imaging techniques because it leads to higher Strehl rations and increased sensitivity. The method will also work when the diffraction limit of the telescope is under-sampled. In that case it can help to improve on the resolution imposed by seeing. Holography can be used with many existing instruments, as long as they provide sufficiently short readout times. Combination of holography and AO imaging provides an interesting perspective for high resolution, high sensitivity images at short wavelengths.

REFERENCES

Blum R. D., Sellgren K., Depoy D. L., 1996, ApJ, 470, 864

Christou J. C., 1991, Experimental Astronomy, 2, 27

Christou J. C., Freeman J. D., Hege E. K., 1987, in J. W. Goad ed., Interferometric Imaging in Astronomy The Weighted Shift-and-Add Method. p. 51

Devillard N., 1997, The Messenger, 87, 19

Diolaiti E., Bendinelli O., Bonaccini D., Close L. M., Currie D. G., Parmeggiani G., 2000, in P. L. Wizinowich ed., Society of Photo-Optical Instrumentation Engineers (SPIE) Conference Series Vol. 4007 of Society of Photo-Optical Instrumentation Engineers (SPIE) Conference Series, StarFinder: an IDL GUI-based code to analyze crowded fields with isoplanatic correcting PSF fitting. pp 879–888

Doucet C., Lagage P., Pantin E., 2006, in V. Coudé du Foresto, D. Rouan, & G. Rousset ed., Visions for Infrared Astronomy, Instrumentation, Mesure, Métrologie High resolution Mid-Infrared Imaging of Dust Disks Structures around Herbig Ae Stars with VISIR. pp 25–30

Eckart A., Genzel R., 1996, Nature, 383, 415

Eckart A., Genzel R., Ott T., Schödel R., 2002, MNRAS, 331, 917

Finger G., Baker I., Dorn R., Eschbaumer S., Ives D., Mehrgan L., Meyer M., Stegmeier J., 2010, in Society of Photo-Optical Instrumentation Engineers (SPIE) Conference Series Vol. 7742 of Society of Photo-Optical Instrumentation Engineers (SPIE) Conference Series, Development of high-speed, low-noise NIR HgCdTe avalanche photodiode arrays for adaptive optics and interferometry

Genzel R., Eckart A., Ott T., Eisenhauer F., 1997, MNRAS, 291, 219

Ghez A. M., Duchêne G., Matthews K., Hornstein S. D., Tanner A., Larkin J., Morris M., Becklin E. E., Salim S., Kremenek T., Thompson D., Soifer B. T., Neugebauer G., McLean I., 2003, ApJ, 586, L127

Ghez A. M., Klein B. L., Morris M., Becklin E. E., 1998, ApJ, 509, 678

Ghez A. M., Morris M., Becklin E. E., Tanner A., Kremenek T., 2000, Nature, 407, 349

Ghez A. M., Salim S., Hornstein S. D., Tanner A., Lu J. R., Morris M., Becklin E. E., Duchêne G., 2005, ApJ, 620, 744

Ghez A. M., Salim S., Weinberg N. N., Lu J. R., Do T., Dunn J. K., Matthews K., Morris M. R., Yelda S., Becklin E. E., Kremenek T., Milosavljevic M., Naiman J., 2008, ApJ, 689, 1044

Gillessen S., Eisenhauer F., Trippe S., Alexander T., Genzel R., Martins F., Ott T., 2009, ApJ, 692, 1075
Hormuth F., Hippler S., Brandner W., Wagner K., Henning T., 2008, in Society of Photo-Optical Instrumentation Engineers (SPIE) Conference Series Vol. 7014 of Presented at the Society of Photo-Optical Instrumentation Engineers (SPIE) Conference, AstraLux: the Calar Alto lucky imaging camera
Kervella P., Verhoelst T., Ridgway S. T., Perrin G., Lacour S., Cami J., Haubois X., 2009, ArXiv e-prints
Knox K. T., 1976, Journal of the Optical Society of America (1917-1983), 66, 1236
Labadie L., Rebolo R., Femenía B., Villó I., Díaz-Sánchez A., Oscoz A., López R., Pérez-Prieto J. A., Pérez-Garrido A., Hildebrandt S. R., Béjar-Sánchez V., José Piqueras J., Rodríguez L. F., 2010, in Society of Photo-Optical Instrumentation Engineers (SPIE) Conference Series Vol. 7735 of Society of Photo-Optical Instrumentation Engineers (SPIE) Conference Series, High spatial resolution and high contrast optical speckle imaging with FASTCAM at the ORM
Labeyrie A., 1970, A&A, 6, 85
Lacour S., Tuthill P., Amico P., Ireland M., Ehrenreich D., Huelamo N., Lagrange A.-M., 2011, A&A, 532, A72
Lenzen R., Hartung M., Brandner W., Finger G., Hubin N. N., Lacombe F., Lagrange A., Lehnert M. D., Moorwood A. F. M., Mouillet D., 2003, in M. Iye & A. F. M. Moorwood ed., Society of Photo-Optical Instrumentation Engineers (SPIE) Conference Series Vol. 4841 of Society of Photo-Optical Instrumentation Engineers (SPIE) Conference Series, NAOS-CONICA first on sky results in a variety of observing modes. pp 944–952
Lohmann A. W., Weigelt G., Wirnitzer B., 1983, Appl. Opt., 22, 4028
Maíz Apellániz J., 2010, A&A, 518, A1+
Mason B. D., Hartkopf W. I., Gies D. R., Henry T. J., Helsel J. W., 2009, AJ, 137, 3358
Ott T., Eckart A., Genzel R., 1999, ApJ, 523, 248
Petr M. G., Coude Du Foresto V., Beckwith S. V. W., Richichi A., McCaughrean M. J., 1998, ApJ, 500, 825
Pott J.-U., Eckart A., Glindemann A., Schödel R., Viehmann T., Robberto M., 2008, A&A, 480, 115
Primot J., Rousset G., Fontanella J. C., 1990, Journal of the Optical Society of America A, 7, 1598
Rengaswamy S., Girard J. H., Montagnier G., 2010, in Society of Photo-Optical Instrumentation Engineers (SPIE) Conference Series Vol. 7734 of Society of Photo-Optical Instrumentation Engineers (SPIE) Conference Series, Speckle imaging with the SOAR and the very large telescopes
Rigaut F. J., Ellerbroek B. L., Flicker R., 2000, in P. L. Wizinowich ed., Society of Photo-Optical Instrumentation Engineers (SPIE) Conference Series Vol. 4007 of Society of Photo-Optical Instrumentation Engineers (SPIE) Conference Series, Principles, limitations, and performance of multiconjugate adaptive optics. pp 1022–1031
Rousset G., Lacombe F., Puget P., Hubin N. N., Gendron E., Fusco T., Arsenault R., Charton J., Feautrier P., Gigan P., Kern P. Y., Lagrange A., Madec P., Mouillet D., Rabaud D., Rabou P., Stadler E., Zins G., 2003, in P. L. Wizinowich & D. Bonaccini ed., Society of Photo-Optical Instrumentation Engineers (SPIE) Conference Series Vol. 4839 of Society of Photo-Optical Instrumentation Engineers (SPIE) Conference Series, NAOS, the first AO system of the VLT: on-sky performance. pp 140–149
Schödel R., 2010, A&A, 509, A260000+
Schödel R., Eckart A., Alexander T., Merritt D., Genzel R., Sternberg A., Meyer L., Kul F., Moultaka J., Ott T., Straubmeier C., 2007, A&A, 469, 125
Schödel R., Merritt D., Eckart A., 2009, A&A, 502, 91
Schödel R., Morris M. R., Muzic K., Alberdi A., Meyer L., Eckart A., Gezari D. Y., 2011, A&A, 532, A83+
Schödel R., Najarro F., Muzic K., Eckart A., 2010, A&A, 511, A18+
Schödel R., Ott T., Genzel R., Eckart A., Mouawad N., Alexander T., 2003, ApJ, 596, 1015
Tuthill P., Lloyd J., Ireland M., Martinache F., Monnier J., Woodruff H., ten Brummelaar T., Turner N., Townes C., 2006, in Society of Photo-Optical Instrumentation Engineers (SPIE) Conference Series Vol. 6272 of Society of Photo-Optical Instrumentation Engineers (SPIE) Conference Series, Sparse-aperture adaptive optics
Weigelt G., Beuther H., Hofmann K., Meyer M. R., Preibisch T., Schertl D., Smith M. D., Young E. T., 2006, A&A, 447, 655
Weigelt G. P., 1977, Optics Communications, 21, 55